Thermal effects on Common Rail injection system hydraulic performance

Thermal effects on Common Rail injection system hydraulic performance

Alessandro Ferrari, Oscar Vento(*)

Energy Department, Politecnico di Torino, corso Duca degli Abruzzi 24, 10129, Torino, Italy

(*) Corresponding author. Email: oscar.vento@polito.it

1. Abstract

The effect of the fuel temperature on the hydraulic performance of a Common Rail diesel injector has been investigated with an integrated experimental-numerical approach. An experimental campaign pertaining to single and double injections has been performed for fuel tank temperatures ranging from 28°C to 68°C. In general, an augment in the injected mass has been observed for increasing values of the fuel tank temperature. Moreover, the interaction between the main and after injection changes with the temperature and the dwell time threshold for fusion-free injections increases with the fuel temperature. The temperature at the injector nozzle has been measured and compared with that obtained with a thermo-fluid dynamics simple model, showing that the real temperature and the estimated one correlate well. The influence of the fuel temperature on the internal injector dynamic has been explored by means of a validated 1D numerical model of the injector thermo-fluid dynamics. The main direct effect of the temperature variation concerns the needle lift, which reaches a larger peak value for a higher fuel temperature: this explains the general increment in the injected mass and the augmented value of the injection fusion threshold for the main-after injections. The obtained results could allow more accurate open-loop control strategies for the injected mass, which include thermal effects, to be implemented.

2. Introduction

The fuel injection apparatus has a key role in a powertrain, since engine efficiency [1], combustion [2] and pollutant emissions [3] are significantly influenced by the injection schedule and for this reason the injection system further development continues to be a research challenge even for alternative fuels.

The Common Rail (*CR*) fuel injection apparatus offers great flexibility in terms of number of injection events per engine cycle, dwell-times between shots and high injection pressure (up to 3000 bar) [4]. The designed shape and quantity of every fuel shot affect combustion and engine-out emission control [5]

and both design parameters, associated to the injector structure [6], and physical factors, such as the fuel properties [7] or the ambient conditions [8], must be taken into account. Fractioning the injection quantity between multiple shots with close-to-zero hydraulic dwell-times according to digital rate shaping strategies, can allow combustion noise to be reduced significantly [9]. An ultra-high injection pressure coupled with small injection holes allow optimal level of fuel atomization, mixture homogeneity and easy evaporation [10]. Soot and hydrocarbon (*HC*) emission reduction can be obtained, thanks to the diminished liquid length and the consequent reduced impingement on walls, and it can be coupled with a NO_x decrease if high EGR rates are simultaneously applied [11]. Besides, an optimal number of orifices and an ideal angular position of them in the nozzle are able to affect the inter- and near-nozzle flow patterns, thus positively affecting lift-off flame and jet interaction with the squish regions [12].

By investigating the influence of low temperature (for both the fuel and the injector body) it has been seen that an injector equipped with a pressure balanced valve shows a pronounced reduction of the fuel injected quantity under cold conditions (the reference temperature was 40 °C for the fuel and 90 °C for the injector body) while a three-way valve injector features negligible differences in the injected mass at 800 bar of rail pressure and a progressive increment of the fuel quantity delivered beyond this rail pressure level [13].

The effect of the injected fuel temperature has been analysed with reference to the spray development and the combustion evolution. For both diesel fuel and DME (dimethyl ether), the higher is the fuel temperature, the earlier is the evaporation and the lower the fuel plume penetration. This causes a lower maximum combustion pressure and a more delayed start of combustion: both these effects lead to a reduction in the NO_x emissions [14, 15]. Furthermore, a reduction in the fuel temperature can cause a higher non-uniformity degree in the fuel-air mixture, which can increase the time necessary to reach a constant level of evaporation rate and can lead to augmented emissions in unburned *HC* [16]. A significant sensitivity of fuel economy and NO_x emission level to the fuel temperature at the injector nozzle has been noticed even for a biodiesel fuelled engine, especially if low EGR rate is used [17].

When a pure biodiesel (B100), characterized by a high viscosity, is considered, the injected fuel temperature can become crucial to improve the biodiesel spray performance. In fact, an increase in the fuel temperature enlarges the spray angle cone and the spray area, which are usually smaller at a fixed temperature if compared with normal diesel fuel. Furthermore, even the pump efficiency improves, due to the reduced viscous friction loses, since fuel viscosity reduces with fuel temperature [18].

The flow through the injection system circuit is not isothermal. The major source of heat input to the fuel in the tank during system working is the fuel recirculated from the injectors [19]. The fuel in the tank reaches the injector inlet after the pumping phase, which determines a temperature increment of about 1 °C every 100 bar of compression [20]. Concerning the temperature evolution within the injector, it has been often predicted in the literature with an isothermal flow assumption [21, 22]. However, with this hypothesis, the temperature rise, due to the viscous dissipation through the injector restrictions and due to the pressure drop, is not simulated [23]. The variations in density, viscosity [21] and bulk modulus [24] with temperature can affect the injector behaviour. In a ballistic injector, where the needle never reaches the upper stroke-end under the usual operating conditions [25], the needle dynamics significantly depends on the pressure and viscous forces which are affected by the temperature [26]. As far as the nozzle holes are concerned, a complex temperature pattern can be identified with 3D numerical simulation, and a separated behaviour between the boundary layer and the core flow is often highlighted. If a 2000 bar injection is considered, the maximum temperature difference in the flow can reach 80 °C between the fluid at the core region and the one at the walls, which is a remarkable value if the temperature dependence of the fuel properties is taken into account [27]. All this highlights a significant role of thermal aspects in the hydraulic performance with effects on the spray.

In the present work, temperature effects on the injector working are analysed. With regard to the hydraulic performance, the temperature at the injector nozzle hole exit has been measured and compared with the one obtained by means of a simple thermodynamic model. Furthermore, a 1D numerical model has been employed to investigate the injector internal dynamics dependence on the fuel temperature. Numerical and experimental tests on single and double injections have been considered in a wide range of nominal rail pressures under different values of the fuel temperature in the tank.

3. Experimental facility

Experimental tests were performed in the Internal Combustion Engines Laboratory at the Politecnico di Torino by means of the Moehwald-Bosch hydraulic test bench for fuel injection systems (maximum speed: 6100 rpm, maximum torque: 100 Nm, nominal power: 35 kW).

The selected calibration fluid is the Shell V-Oil 1404 (ISO 4113) since it is capable to satisfactorily reproduce diesel oil properties up to 150 °C over the entire pressure range.

Tests were conducted on a Bosch CR injection system for a 4 cylinders passenger car diesel engine. A high-pressure rotary pump, featuring a displacement of 430 mm^3/rev and a double effect single piston, is

employed to feed the rail. The rail is connected with solenoid-actuated CRI 2.18 injectors, a scheme of which is reported in Fig. 1. The high-pressure fuel enters the injector and a part of it reaches the delivery chamber (volume V_{dc}) upstream the nozzle zone, and the other part, through the Z hole, fills the control chamber (volume V_{cc}). As soon as the electrical current supplied by the Electronic Control Unit (ECU) is switched on, the injector solenoid is energized and the control chamber discharges fuel from the pilot valve through the A hole. Therefore, the pressure forces acting on the needle become unbalanced and the latter moves up, opening the nozzle and allowing the fuel injection. When the ECU switches off the current to the solenoid, the closure of the pilot valve makes the pressure rise in the control chamber, therefore the needle starts its closure phase, which finishes when its tip touches the seat. Hence, the nozzle is again closed and injection ends [9]. The injected fuel quantity depends on both the time-averaged value of the injection pressure and on the hydraulic duration of the injection, which is related to the electrical command to the solenoid, i.e. the energizing time (*ET*) [28].

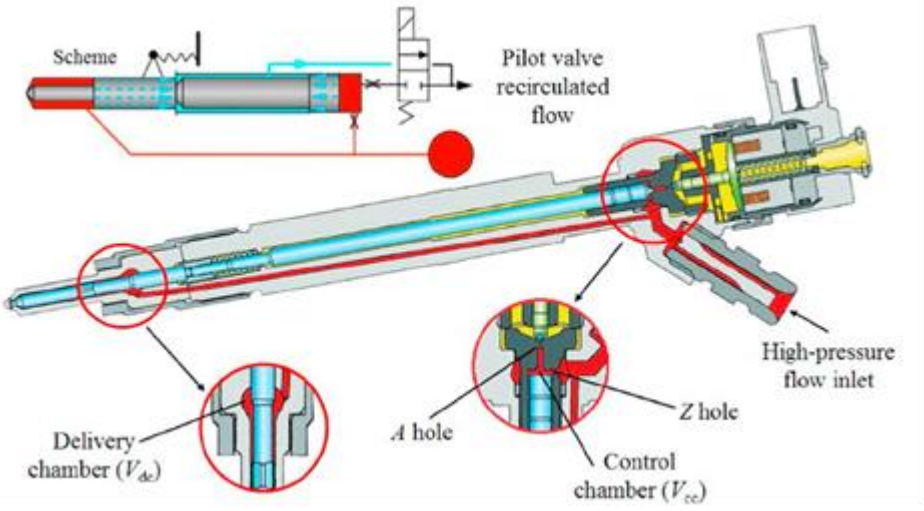

Figure 1. CRI 2.18 injector.

A piezoresistive transducer has been mounted at the injector inlet along the rail-to-injector pipe to measure the pressure time history ($p_{inj,in}$) and this datum will be used as a boundary condition for the numerical model. The transducer measuring range is up to 2000 bar and its linearity error is lower than ±0.1% of the fuel scale value. It has been assumed that the only uncertainty contribution that affects the transducer accuracy is the linearity error, which is lower than ±2 bar.

The injected flow-rate and the injected mass have been measured by means of the HDA flowmeter. In this instrument the pressure in a closed volume is measured, together with the speed of sound (for which

an ultrasonic sensor is employed), then, by following Zeuch's method, the injected mass flow-rate is obtained [29].

The fuel temperature at the nozzle hole exit has been measured by means of a PT100 temperature sensor mounted at a distance of 25 mm from the injector tip along a duct with a counterpressure of 40 bar where the fuel is injected. The same injector previously mounted in the HDA to detect the injected flow-rate has then been made inject the fuel in the pipe with the PT100 sensor to measure the fuel temperature under the same controlled working conditions.

Single injections, together with pilot-main and main-after injections, have been considered in this research investigation. Tests have been performed by varying the *ET* at different nominal rail pressure (p_{nom}) values for single injections, while for double injections the *ET* values for the considered injections have been kept constant and the dwell time between the shots has been varied. The fuel temperature at the pump inlet was varied from 28 °C to 68 °C. In particular, 28°C represents the minimum value that can be controlled by the current test bench, 40 °C is usually assumed as the reference temperature for hydraulic tests by the fuel injection system manufacturers and 68 °C represents the maximum temperature that can be reached on the test bench for safety reasons. The hydraulic test bench can heat the fuel in the tank by means of a heating coil and, at the pump inlet, the fuel temperature is controlled by means of a heat exchanger where the cooling water flowrate is regulated in order to fulfil the fuel temperature requirement (the fuel temperature at the pump inlet is measured by means of a temperature probe that represents the feedback signal to modify the cooling water flowrate). Tests have been performed at a pump speed of 2000 rpm.

4. Fuel properties and temperature in the injection apparatus

The temperature can affect the fuel properties significantly. The ones here considered are the density (ρ), the bulk modulus (E), the dynamic viscosity (μ) and the thermal expansivity (β), which is defined as $-\frac{1}{\rho}\left(\frac{\partial \rho}{\partial T}\right)_p$. Figure 2 reports the trends of the ISO 4113 oil properties, experimentally determined, as functions of the temperature for different nominal rail pressures, according to [21]: symbols stand for the experimental values, whereas the solid lines correspond to the determined polynomial interpolating expressions.

The test rig can control the tank oil temperature (T_{tank}). By assuming an isentropic evolution of the fuel through the pump compression, the temperature increase, due to the pressure rise, can be estimated.

If the fundamental thermodynamic state relation [30] is considered for an isentropic compression, one has:

$$dh = \frac{dp}{\rho} \qquad (1)$$

where h is the enthalpy per unit of mass. For a liquid, the enthalpy is defined as:

$$dh = c_p dT + (1 - \beta T)\frac{dp}{\rho} \qquad (2)$$

where c_p is the specific heat at constant pressure. By combining Eqs. (1) and (2), one obtains:

$$c_p dT = \beta T \frac{dp}{\rho} \qquad (3)$$

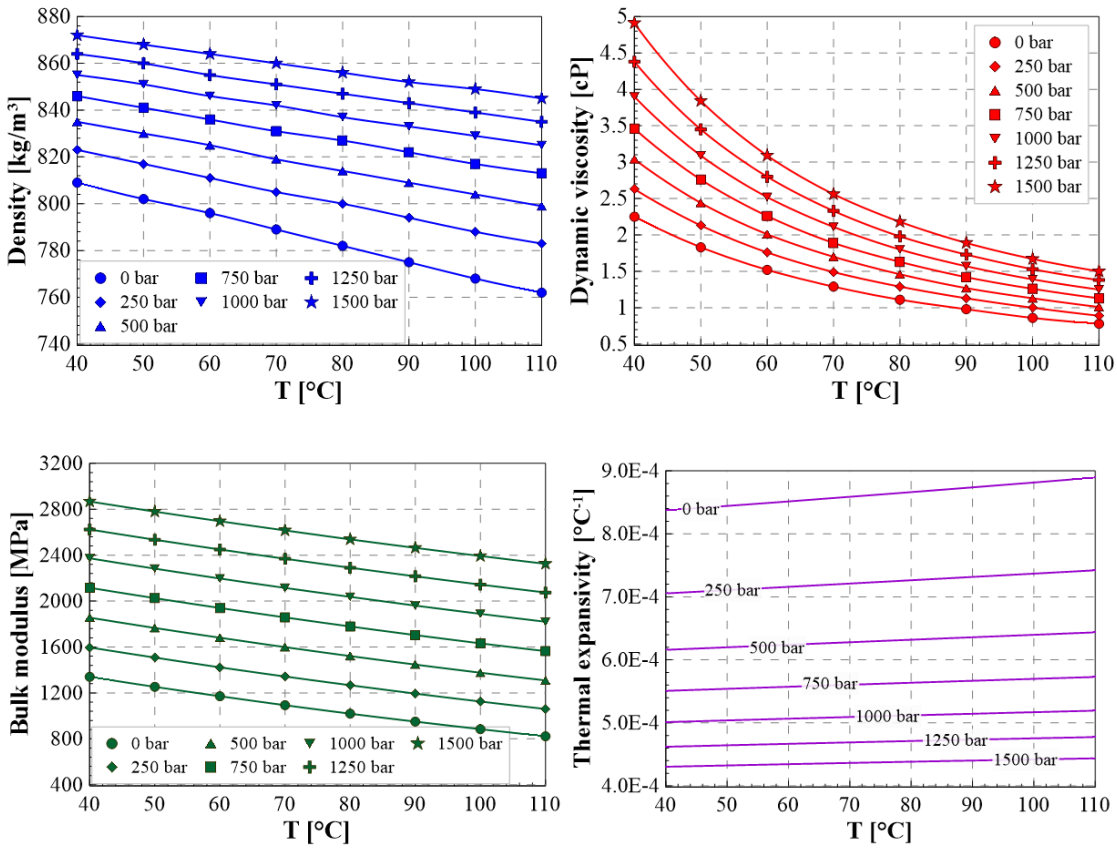

Figure 2. ISO 4113 oil properties with respect temperature and pressure.

Hence an estimation of the temperature level in the high-pressure circuit can be obtained for a certain nominal rail pressure.

The fuel temperature through the injector can be estimated by considering an isenthalpic evolution [21], if the injector is roughly regarded as a set of localized restrictors. The injected fuel temperature can therefore be predicted as follows:

$$c_p dT = (\beta T - 1)\frac{dp}{\rho} \qquad (4)$$

5. Experimental results

Figure 3 reports the trend of the fuel temperature measured at the nozzle hole exit with respect to *ET*; data refers to p_{nom}= 800 bar and to both T_{tank}= 40 °C and T_{tank}= 68 °C. Tests were also performed at T_{tank}= 28°C and measure fuel temperatures resulted slightly lower than the corresponding ones at T_{tank}= 40 °C. After a certain value of *ET*, the measured temperature reaches an asymptotic value. This can be interpreted by considering the measuring procedure used to obtain the temperature value. When *ET* is small, the injected flow-rate is not high enough to let the sensor measure a steady-state temperature in the pipe where the fuel is injected. Therefore, if the *ET* is increased, the detected temperature augments and finally reaches an asymptotic value, which is the steady-state one that should be considered in the comparison with the isenthalpic model. The asymptotic values measured for different nominal rail pressures (cf. Fig. 3) have been adopted as the fuel temperatures at the nozzle outlet in the numerical simulations.

In Fig. 4, the measured oil temperature at the nozzle exit for *ET*=3000 μs is plotted (with symbols) with respect to the correspondent isenthalpic temperature obtained for a certain rail pressure under the adiabatic assumption, for both T_{tank} = 40 °C and T_{tank} = 68 °C. Although the curves are well distinct from the bisector and the isenthalpic assumption overestimates the real temperature (the injector is less dissipative than a restrictor) the estimations provided can be reasonable. Furthermore, the experimental and isenthalpic temperatures are well correlated, and the correlation is almost linear (cf. the continuous lines in Fig. 4). Hence, for a fixed T_{tank} and a given rail pressure level, the isenthalpic temperature at the nozzle can be obtained by means of Eq. (4) and a more accurate estimation of the real temperature can be obtained by means of a correlation curve which can be determined for each injector typology.

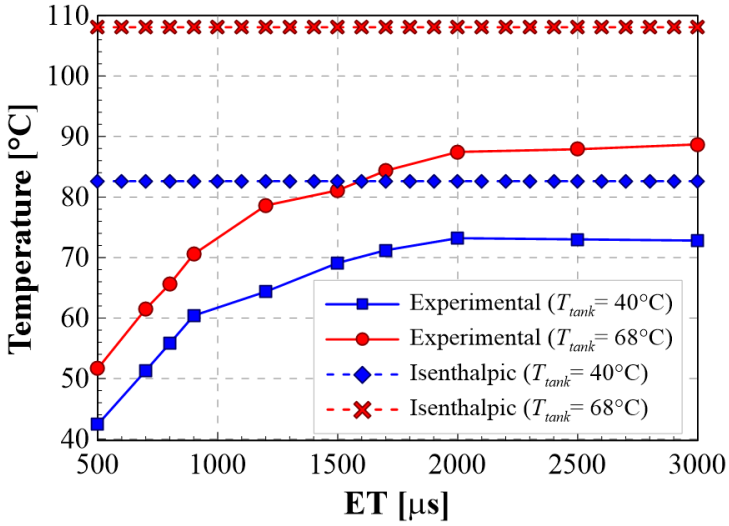

Figure 3. Fuel temperature at the injector exit for different ET and T_{tank} values (p_{nom} = 800 bar).

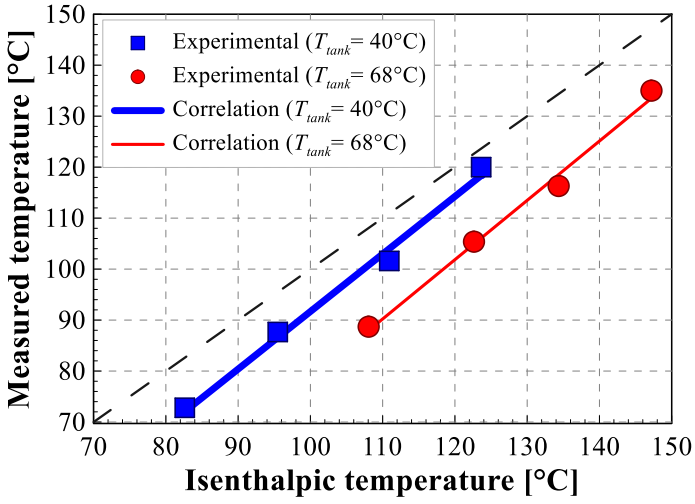

Figure 4. Correlation between the measured temperature at the injector outlet and the isenthalpic temperature.

Tests for single injections have been performed over a wide range of nominal rail pressure (between 600 bar and 1800 bar) and of *ET* (between 350 μs and 1000 μs) in order to explore the entire range of working conditions for a diesel passenger car. Figure 5 shows the injector characteristics pertaining to different nominal rail pressure levels and to two distinct fuel tank temperatures, namely 40 °C and 68 °C. As can be inferred from Fig. 5, the injected mass generally increases with the fuel temperature for a fixed working condition in terms of p_{nom} and *ET*.

Figure 6 reports the injected flow-rates for p_{nom}=1600 bar and *ET*= 600 μs, at two different T_{tank} values. It can be observed that the injection temporal length (*ITL*) increases with the tank fuel temperature, and this leads to an augmented injected fuel quantity for fixed *ET* and p_{nom}. [31].

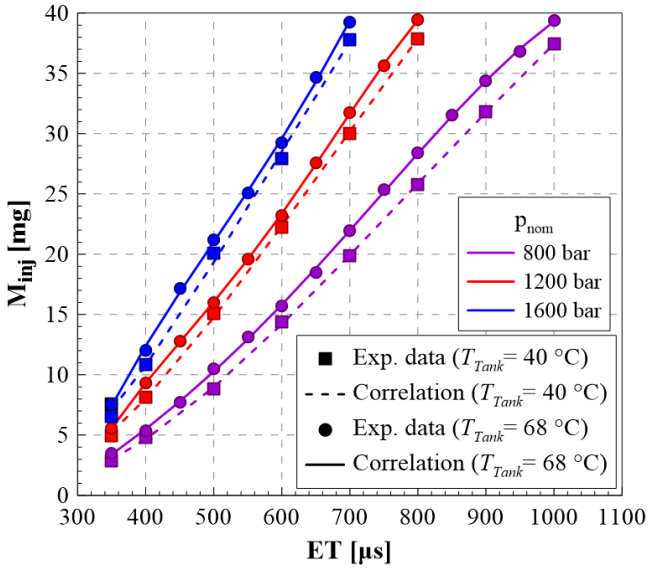

193

194 **Figure 5. Injector characteristics for different nominal rail pressure levels and fuel tank temperatures.**
195

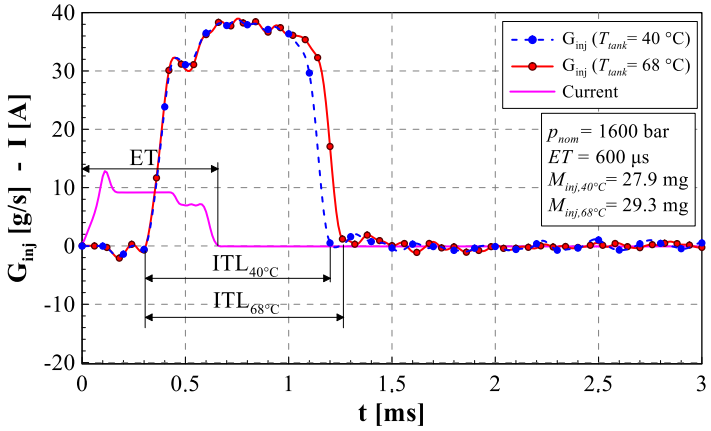

196

197 **Figure 6. Injected flow-rate for different fuel tank temperature values (pnom = 1600 bar, ET = 600 µs).**
198

199 As far as the double injections experimental campaign is concerned, a CRI 2.20 injector has been
200 employed. This injector, differently from the CRI 2.18 used for the analysis on single injections, features
201 a Minirail in place of the delivery chamber (the latter corresponds to volume V_{dc} in Fig. 1) in order to
202 reduce the injected mass fluctuation of the second shot with respect to the dwell time [25]. It has been
203 already verified that also the CRI 2.20 injector is affected by a thermal drift similar that of the CRI 2.18
204 injector, and an augment in the injected mass can be detected as the fuel temperature increases [31].
205 Pertaining to pilot-main injections, a *DT* sweep has been reported in Fig. 7, referring to p_{nom}= 800 bar,
206 ET_{pil} = 230 µs and ET_{main} = 500 µs. The overall injected mass $M_{inj,total}$ (given by the sum of pilot and main
207 injected masses), measured by means of the HDA, has been reported at different *DT* values for both T_{tank}
208 = 40°C (blue curve) and T_{tank} = 68°C (red curve). The injected mass increases with the temperature, as

occurs for single injections, while the dynamic features of the system, such as the injection fusion threshold, do not vary appreciably.

Regarding main-after injections, the overall injected mass with respect to the dwell time value is represented in Figure 8 for the case p_{nom}= 1400 bar, ET_{main} = 400 µs, ET_{aft} = 200 µs at two different fuel tank temperatures, i.e. T_{tank} = 40°C (blue curve) and T_{tank} = 68°C (red curve). The most evident effect is, even in this case, an augment in the injected mass when the fuel temperature increases. Moreover, it can be observed that the injection fusion threshold, that is the minimum dwell-time value for which two injections are still hydraulically distinct, increases with the temperature. This is obvious in Figure 9, where the injected flowrates for the *DT* = 540 µs case is reported for both T_{tank} = 40°C (blue curve, the main and after injection are still separated), and T_{tank} = 68 °C, (red curve, where the needle never closes the nozzle holes during the entire injection event).

Many strategies can be implemented on the ECU to correct the injection schedules in order to compensate for the abovementioned fuel temperature effects. As an example, the main energizing time can be modified according to the engine water cooling temperature, by means of on an open-loop strategy, through an empirical coefficient. The presented thermo-fluid dynamic model allows the temperature of the injected fuel, which considers the temperature increase due to both the fuel compression in the high-pressure pump and the fuel expansion across the injector, to be used to refine the open-loop control strategy of the injected mass.

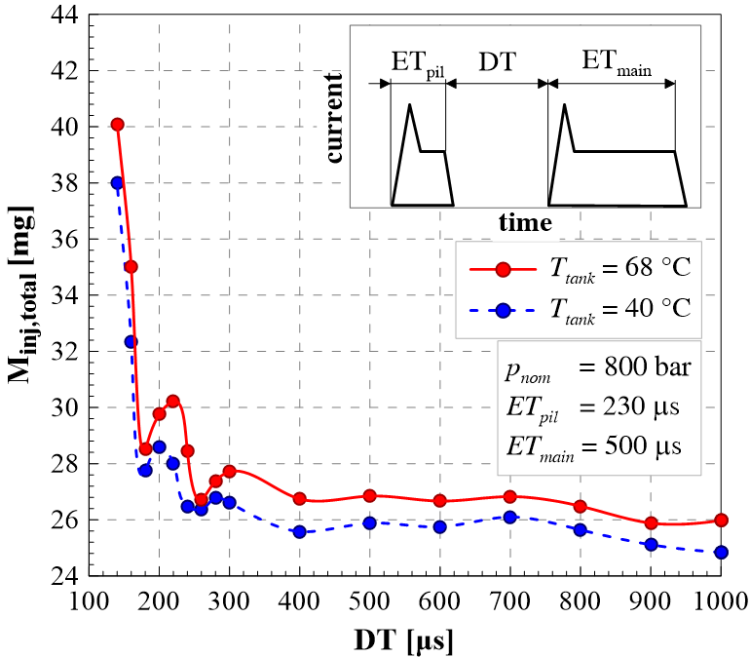

Figure 7. Pilot-main injection *DT* sweep for different fuel tank temperatures.

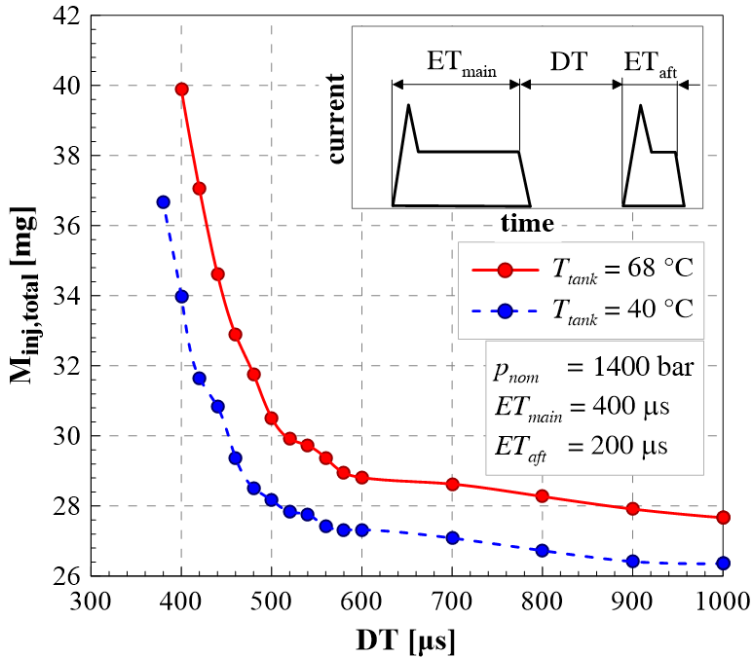

Figure 8. Main-after injection *DT* sweep for different fuel tank temperatures.

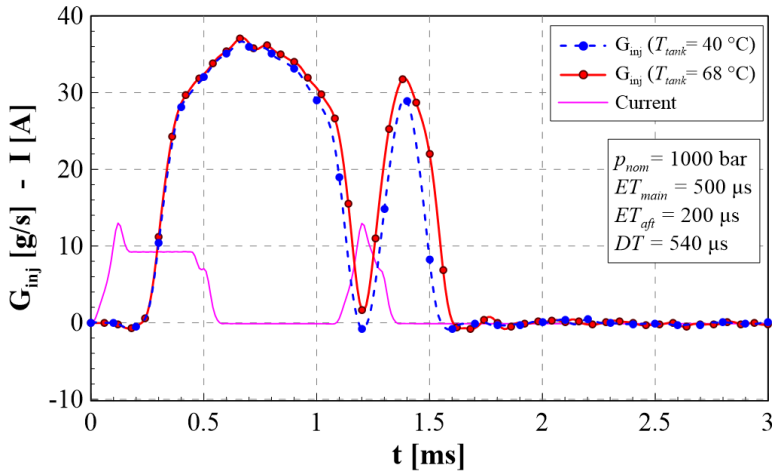

Figure 9. Injected flow-rate for a main-after injection for different fuel tank temperatures.

6. Model description

The analysis regarding single injection is based on a 1D injector numerical diagnostic tool developed in [32, 33] and further validated at different fuel temperatures. A scheme of the 1D model is represented in Fig. 10. The circuit generally consists of a network of 0D chambers connected by means of 1D pipes [34]. The boundary conditions consist of the measured pressure time history at the injector inlet along the rail-to-injector pipe and of the electrical current signal provided to the solenoid of the pilot valve. By selecting these boundary conditions, any inaccuracy, due to the modelling of the rail, the injector feeding pipe, the pump and the ECU, can be avoided.

During the needle movement, a viscous force is generated between the needle and the injector body, due to the presence of a thin boundary layer. The flow in the small annular passage (cf. Fig. 10) is laminar and follows Poiseuille's law. The viscous friction force in this zone can therefore be evaluated as [35]:

$$F_{fric} = \frac{\mu \cdot L_c \cdot v \cdot \pi \cdot d_n}{\delta_r} \quad (5)$$

where d_n is the needle diameter, L_c represents the length of the annular passage, δ_r is the radial distance between the needle and the injector holder and v is the velocity of the needle.

The needle movement is related to the pressure variation in the control chamber, that is to the control chamber discharge and refilling through the A and Z holes, respectively (cf. Fig. 10). The Z hole is in a non-cavitating condition, whereas the A hole can experience cavitation conditions [36]. One important point in thermal models concerns the discharge coefficient of the holes.

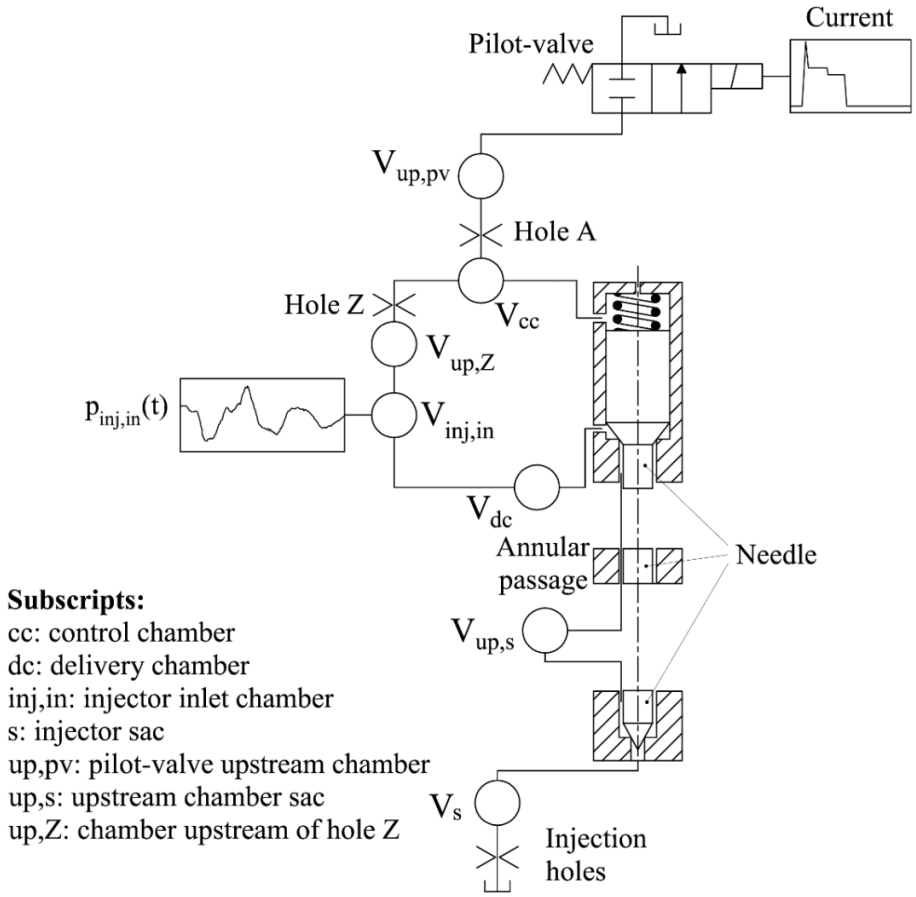

Figure 10. Scheme of the 1D numerical model.

The discharge coefficient of a hole is defined as the ratio of the effective flow-rate to the ideal one, obtained by means of the Bernoulli equation for a liquid flow [37].

For a cavitation-free hole the discharge coefficient C_d has been defined as follows [38]:

$$C_d = C_{d,max} \cdot tanh\left(\frac{2 \cdot Re}{Re_{crit}}\right) \quad (6)$$

where $C_{d,max}$ is the maximum value of the discharge coefficient, Re is the Reynolds number and Re_{crit} is the critical Reynolds number, where the transition between laminar and turbulent flow occurs. The Reynolds number is calculated in the following way:

$$Re = \frac{D}{\mu} \cdot \sqrt{2\Delta p \rho} \quad (7)$$

where D is the hole diameter and Δp the pressure drop across the hole.

When the flow through the hole can be subjected to cavitation phenomena, the cavitation number CN can be introduced [39]:

$$CN = \frac{p_{in} - p_v}{p_{in} - p_{out}} \quad (8)$$

where p_{in}, p_{out} and p_v are the pressure value at the inlet of the hole, at the outlet of the hole and the vapour pressure of the fuel, respectively. When CN is lower than a critical cavitation number (CN_{crit}) which is experimentally obtained, cavitation occurs, and the discharge coefficient is calculated by considering the actual cavitation number CN and the contraction coefficient C_c according to this expression [40]:

$$C_d = C_c \cdot \sqrt{CN} \quad (9)$$

In the present investigation, the flow coefficient pertaining to Z hole was evaluated with Eqs. (6) and (7), whereas the complete model of C_d which includes Eqs. (6-9) was implemented for A hole and for the injection holes in order to simulate possible cavitation occurrences.

6.1 Numerical model results

Figure 11 shows the comparison between the experimental injected flow-rates (plotted with symbols) and the numerical ones (plotted with continuous line) for the two pressure levels 800 bar (Fig. 11a), and 1700 bar (Fig. 11b). The T_{tank} was set at 40°C and the results pertaining to different ETs have been reported in the plots. The corresponding results referring to T_{tank} = 68 °C have been plotted in Fig. 12. It can be observed that the numerical results match the experimental ones accurately.

In Fig. 13, the numerical control chamber pressure traces have been reported for both T_{tank} = 40 °C and T_{tank}= 68 °C (p_{nom}= 800 bar and ET= 800 µs). As can be inferred, the difference in fuel temperature does not affect significantly the pressure time history in the control chamber because both the flow-rates

through the Z and A holes are almost the same for the two cases. This is in line with the results available in the literature, where the effect of the fuel temperature on the control chamber pressure and flow-rates through A and Z holes are significant only when the fuel temperature within the injector is below 0° C [36]. From the numerical model it results that the A hole is experiencing cavitating condition for both the tested T_{tank} temperatures and only a small increase in the *CN* can be noticed for T_{tank} = 40°C, leading to a slight augment in the C_d value. Instead, the Z hole doesn't undergo any cavitating regime and the flow is turbulent for both T_{tank} = 40°C and T_{tank} = 68 °C.

Figure 14 reports the numerical pressure time histories detected in the delivery chamber (p_{dc}), in the upstream-sac chamber ($p_{up,s}$) and in the injector sac (p_{sac}) (cf. Fig. 10 for the chambers location), as well

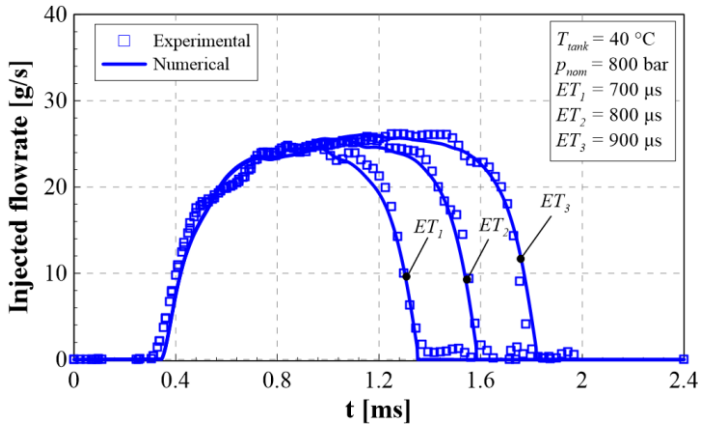

(a)

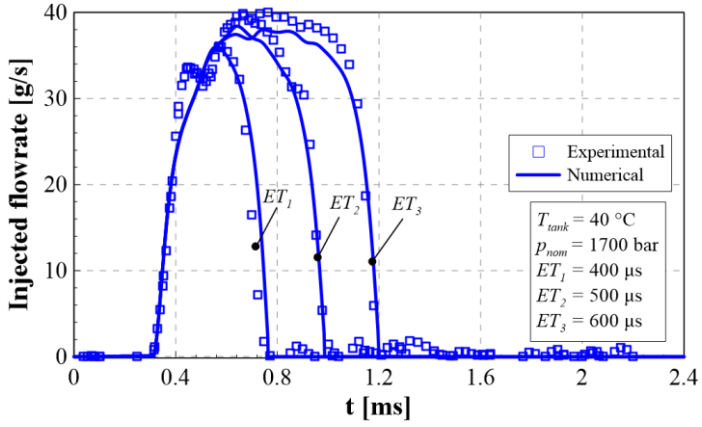

(b)

Figure 11. Experimental injected flow-rates compared with the numerical ones with T_{tank} = 40 °C, p_{nom} = 800 bar (a), p_{nom} = 1700 bar (b).

as the needle lift numerical trace (p_{nom}=800 bar, *ET*=1000 us, T_{tank}=40 °C). The temperature at the injector inlet (cf. $V_{inj,in}$ in Fig. 10) is provided as an input datum to the injector model and has been obtained by means of Eq. (3). For the other injector chambers, starting from the injector inlet temperature, the

instantaneous pressure difference between two adjacent chambers (cf. $\Delta p_{dc\rightarrow up,s}$, $\Delta p_{up,s\rightarrow sac}$ and $\Delta p_{sac\rightarrow cyl}$ in Fig. 14) is used to estimate the temperature rise under the *h=const* hypothesis and, by means of the correlation reported in Fig. 4, an estimation of the real temperature can be obtained. If the isenthalpic temperature results to be outside from the considered range in Fig. 4, a linear extrapolation has been performed. In fact, based on data of fuel temperature measured at the nozzle exit for a wide range of p_{nom} values in [41], it was possible to extend the linear correlations reported in Fig. 4 up to about 160 °C (for T_{tank}= 40 °C) and to about 180 °C (for T_{tank}= 68 °C).

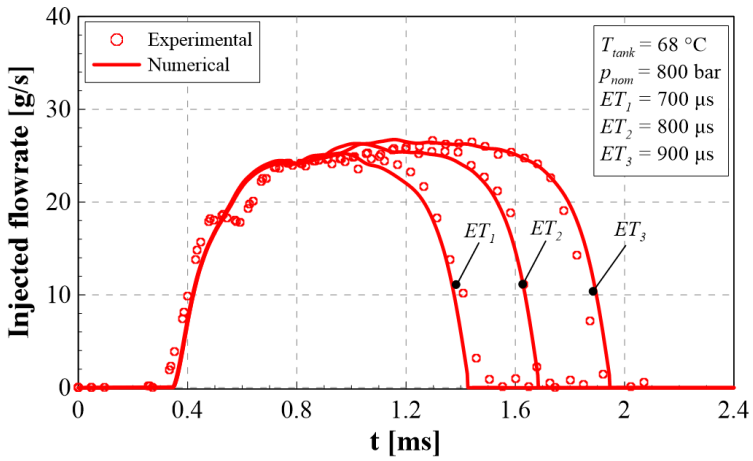

(a)

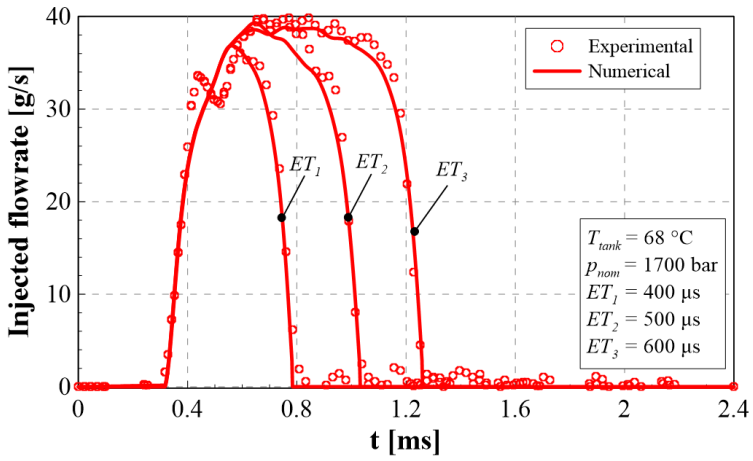

(b)

Figure 12. Experimental injected flow-rates compared with the numerical ones with with T_{tank} = 68 °C, p_{nom} = 800 bar (a), p_{nom} = 1700 bar (b).

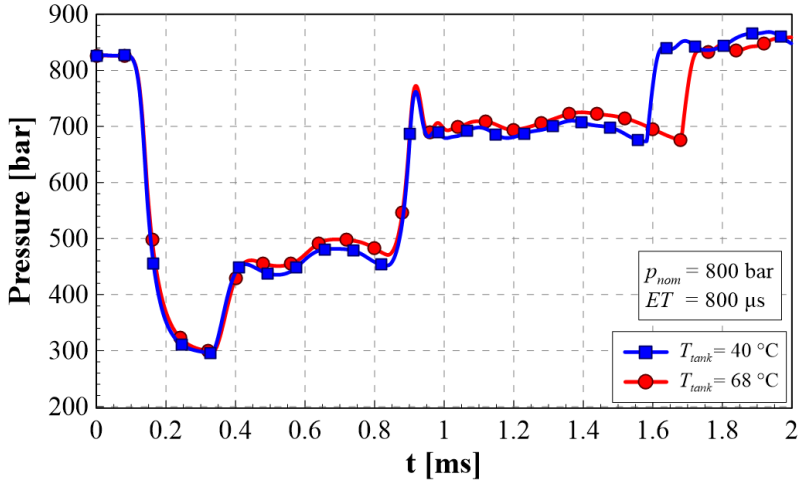

Figure 13. Pressure in the control chamber for T_{tank} = 40 °C and 68 °C, p_{nom} = 800 bar, ET= 800 µs .

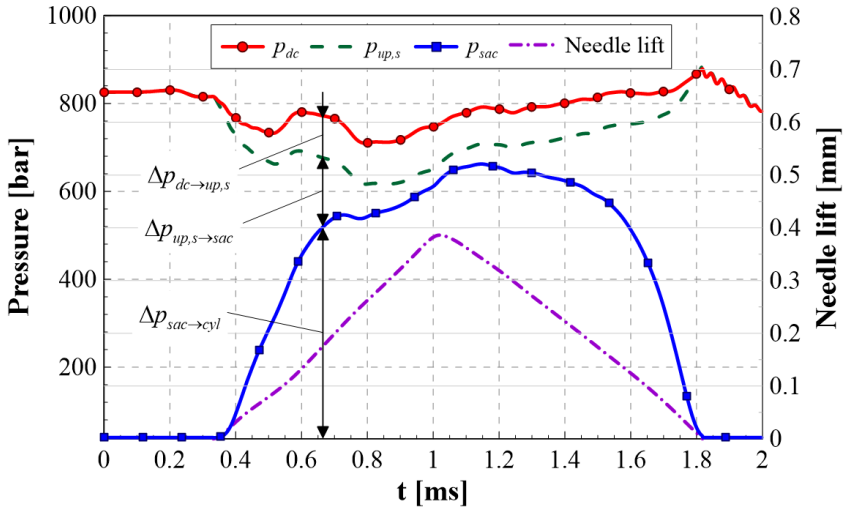

Figure 14. Pressure time histories and needle lift from the numerical model, p_{nom} = 800 bar, ET= 800 µs, T_{tank} = 40 °C.

At the beginning and at the end of the injection event, the pressure drop $\Delta p_{up,s\rightarrow sac}$ is larger than $\Delta p_{sac\rightarrow cyl}$ (cf. Fig. 14) because the restricted flow area is at the needle-seat passage. Therefore, the fuel heating phase mainly occurs when the fuel flows across the passage between the needle and its seat. On the other hand, when the needle lift is sufficiently high and the flow-rate is controlled by the nozzle holes, $\Delta p_{sac\rightarrow cyl}$ becomes much larger than $\Delta p_{up,s\rightarrow sac}$, hence the fuel heating mainly occurs through the nozzle holes.

In Fig. 15 the numerical needle lift time distribution is reported, for both the considered T_{tank} temperatures, together with the numerical injected flow-rates (p_{nom} = 800 bar, ET = 800 µs). Figure 16 plots the same quantities as in Fig. 15 but with reference to a different working condition (p_{nom} = 1700 bar, ET = 600 µs).

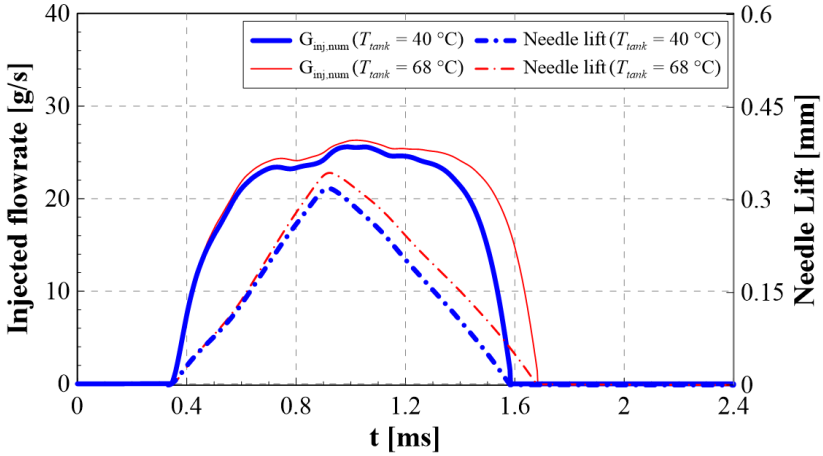

Figure 15. Injected flowrate and needle lift for T_{tank} = 40 °C and 68 °C, p_{nom} = 800 bar, ET= 800 µs .

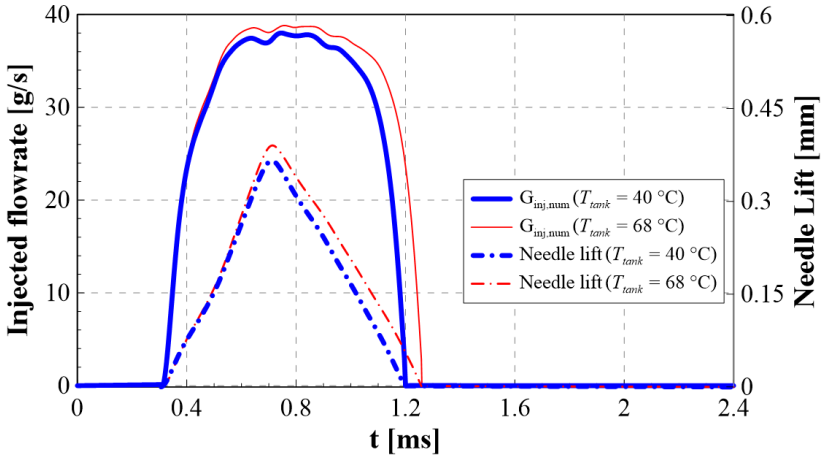

Figure 16. Injected flowrate and needle lift for T_{tank} = 40 °C and 68 °C, p_{nom} = 1700 bar, ET= 600 µs .

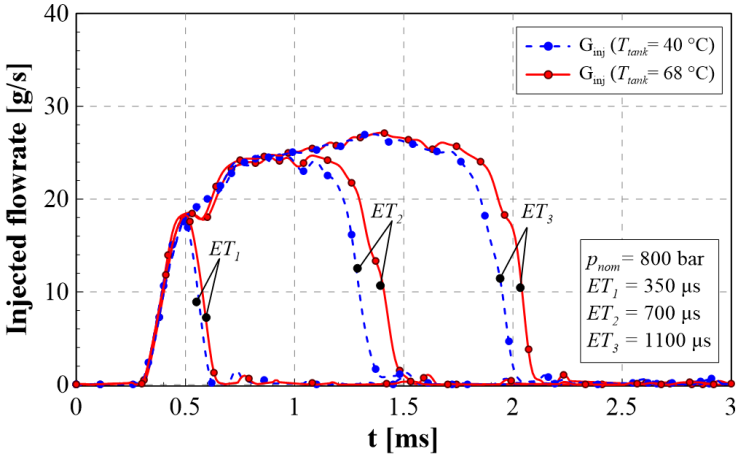

Figure 17. Injected flow-rates for different ET values with T_{tank} = 40 °C and 68 °C, p_{nom} = 800 bar.

In general, since the fuel viscosity reduces with the temperature (the decreasing trend is exponential in Fig. 2), the viscous force acting on the needle diminishes as the fuel temperature augments. Therefore,

due to the reduced viscous force, the needle velocity increases during the opening phase as T_{tank} augments, leading to a higher needle peak lift value under a fixed *ET*. Then, after the electrical current is switched off, the needle starts its closure phase and, the higher is the temperature, the larger is the needle downstroke required to close the nozzle, and therefore the longer are the nozzle closure delay and the injection duration.

The effect of the fuel temperature is less obvious for injections characterized by small *ETs*, as is shown in Fig. 17. In fact, a shorter-*ET* injection is characterized by a smaller needle lift peak value and the absolute variation of the latter with T_{tank} is small. Hence, the higher is the needle lift peak value, the more evident is the effect of the fuel temperature in the final part of the injected flow-rate.

In [36] it has been verified that, even for a CRI 2.20 injector, the main effect of the fuel temperature, in the considered range, is given by a reduced viscous force acting on the needle, which leads to a higher needle lift peak. Therefore, for the pilot-main injections, the higher needle lift peak obtained at higher fuel temperature leads to a general increment in the mass, although the injection fusion threshold does not change considerably, as shown in Fig. 7. Instead, for main-after injections, when the tank fuel temperature grows, an augment in the injection fusion threshold can be detected, together with an increment in the injected mass (cf. Figs. 8-9). The injection fusion threshold increment is justified, since the tendency to reach higher needle-lift peak values for larger fuel temperatures becomes more evident for longer injections (cf. Fig 17): unlike pilot-main schedules, the shot with the larger *ET* is the former in main-after injections.

7. Conclusions

The fuel temperature effect on the hydraulic performance of a CR injection system has been analyzed by means of both experimental and numerical results. The major findings can be summarized as follows:

- the experimental campaign on single and double injections (pilot-main and main-after schedules) has shown that, when the fuel temperature increases, the injected mass generally grows. Furthermore, the fuel temperature appreciably affects the injection fusion threshold of the main-after injections;
- the injected fuel temperature has been measured along a pipe where the fuel is injected, at a distance of 25 mm from the injector tip. This experimental temperature has been compared successfully with the one obtained by means of a newly developed simple thermo-fluid dynamics model: starting from the fuel tank temperature, and by considering an isentropic compression through the pump, the fuel temperature

at the injector entrance has been obtained. Furthermore, by means of an isenthalpic evolution assumption across the injector, the final temperature at the nozzle exit has been calculated;

- a 1D numerical model has been used to investigate the injector dynamics at different fuel temperatures. The most relevant effect of the fuel temperature increase is the reduction in the fuel viscosity, which leads to a diminished viscous force that acts against the needle movement. When the fuel temperature increases, the needle reaches an augmented peak value, which explains the experimental differences with respect to the fuel temperature for both single and double injections;

- the 1D numerical model shows that the fuel heating inside the injector occurs primarily in correspondence of the needle seat passage, with an effect on the beginning and end of the injection law, as well as across the nozzle holes with an effect on the central part of the injection law;

- an innovative open-loop control strategy of the injected mass, based on the estimated nozzle exit fuel temperature, could be designed to improve the compensation of the injector thermal drifts during engine operation (the current strategies are usually based on the water cooling temperature).

8. References

[1] Beatrice, C., Di Blasio, G., Pesce, F.C., Vassallo, A. et al., "Key Fuel Injection System Features for Efficiency Improvement in Future Diesel Passenger Cars," *SAE Int. J. Advances & Curr. Prac. in Mobility* 1(3):1084-1099, 2019.

[2] Yang F, Yao C, Wang J, Ouyang M. "Load expansion of a dieseline compression ignition engine with multi-mode combustion". *Fuel* 2016;171:5‑17.

[3] Vakiti, K., Deussen, J., Pilger, C., Nanjundaswamy, H., Szailer, T., Franke, M., Tomazic, D., Thomas, K., Romijn, M., Deppenkemper, K., and Vagnoni, G. "In-Use Compliance Opportunity for Diesel Powertrains," SAE Technical Paper 2018-01-0877, 2018.

[4] Boccardo, G., F. Millo, A. Piano, L. Arnone, S. Manelli, Simon Fagg, P. Gatti, Olaf E. Herrmann, Dirk Queck and Jost Weber. "Experimental investigation on a 3000 bar fuel injection system for a SCR-free non-road diesel engine." *Fuel* 243 (2019): 342-351.

[5] Niculae AL, Chiriac R, Racovitza A. Effects of Injection Rate Shape on Performance and Emissions of a Diesel Engine Fuelled by Diesel and Biodiesel B20. *Applied Sciences*. 2022; 12(3):1333. https://doi.org/10.3390/app12031333

[6] Kang, S., Lee, S., Hong, D., & Bae, C. (2022). Effects of Nozzle Orifice Diameter and Hole Number on Diesel Combustion and Engine Performance. *International Journal of Automotive Technology*, *23*, 481-494.

[7] Liu, H., Ma Jun-sheng, F. Dong, Y. Yang, X. Liu, Ma Gui-xiang, Z. Zheng and M. Yao. "Experimental investigation of the effects of diesel fuel properties on combustion and emissions on a multi-cylinder heavy-duty diesel engine." *Energy Conversion and Management* 171 (2018): 1787-1800.

[8] Ma, Y., L. Cui, X. Ma and J. Wang. "Optical study on spray combustion characteristics of PODE/diesel blends in different ambient conditions." *Fuel* 272 (2020): 117691.

[9] Ferrari, A., C. Novara, E. Paolucci, O. Vento, M. Violante and T. Zhang. "A new closed-loop control of the injected mass for a full exploitation of digital and continuous injection-rate shaping." *Energy Conversion and Management* 177 (2018): 629-639.

[10] Zhai, C., Jin, Y., Wu, Q., Nishida, K., & Ogata, Y. (2021). Diesel spray and combustion of multi-hole injectors with micro-hole under ultra-high injection pressure – Combustion characteristics. *Fuel, 300*, 120949.

[11] Wang, Xiangang, Zuohua Huang, W. Zhang, O. Kuti and K. Nishida. "Effects of ultra-high injection pressure and micro-hole nozzle on flame structure and soot formation of impinging diesel spray." *Applied Energy* 88 (2011): 1620-1628.

[12] Moon, S., Y. Gao, S. H. Park, J. Wang, N. Kurimoto and Y. Nishijima. "Effect of the number and position of nozzle holes on in- and near-nozzle dynamic characteristics of diesel injection." *Fuel* 150 (2015): 112-122.

[13] Cavicchi, A., Postrioti, L., Pesce, F.C., and Ferrara, U., "Experimental Analysis of Fuel and Injector Body Temperature Effect on the Hydraulic Behavior of Latest Generation Common Rail Injection Systems," SAE Technical Paper 2018-01-0282, 2018, doi:10.4271/2018-01-0282.

[14] Kubota, Masaru, K. Yoshida, H. Shoji and H. Tanaka. "8 A Study of the Influence of Fuel Temperature on Emission Characteristics and Engine Performance of Compression Ignition Engine." SAE Technical Paper. (2002).

[15] Guangxin, Gao, Y. Zhu-lin, Zhou Apeng, Liu Sheng-hua and Wei Yanju. "Effects of Fuel Temperature on Injection Process and Combustion of Dimethyl Ether Engine." *Journal of energy resources technology* 135 4 (2013): 422021-422025 .

[16] Babadi, M. N., S. Kheradmand and C. Bae. “Experimental and Computational Investigation of Diesel and Gasoline Injection in a Direct Injection Compression Ignition Engine.” *International Journal of Automotive Technology* 21 (2020): 23-32.

[17] Mamat, R., Abdullah, N. R., Xu, H., Wyszynski, M. L., & Tsolakis, A. (2009). *Effect of fuel temperature on performance and emissions of a common rail diesel engine operating with rapeseed methyl ester (RME)* (No. 2009-01-1896). SAE Technical Paper.

[18] Anis, Samsudin and Galuh Nur Budiandono. “Investigation of the effects of preheating temperature of biodiesel-diesel fuel blends on spray characteristics and injection pump performances.” *Renewable Energy* 140 (2019): 274-280.

[19] El-Sharkawy, A., "Transient Thermal Analysis of Diesel Fuel Systems," *SAE Int. J. Mater. Manf.* 5(2):2012, doi:10.4271/2012-01-1049.

[20] A. Ferrari, Z. Jin, O. Vento, T. Zhang. An injected quantity estimation technique based on time–frequency analysis. Control Eng Pract, 116 (2021), 104910

[21] Catania, A., Ferrari, A., Manno, M., and Spessa, E., “Thermal Effect Simulation in High-Pressure Injection System Transient Flows,” SAE Technical Paper 2004-01-0532, 2004.

[22] Payri, R., Salvador, F.J., Carreres, M., and Belmar-Gil, M., “An Investigation on the Fuel Temperature Variations Along a Solenoid Operated Common-Rail Ballistic Injector by Means of an Adiabatic 1D Model,” SAE Technical Paper 2018-01-0275, 2018.

[23] Salvador, F., J. Gimeno, M. Carreres and M. Crialesi-Esposito. “Experimental assessment of the fuel heating and the validity of the assumption of adiabatic flow through the internal orifices of a diesel injector.” *Fuel* 188 (2017): 442-451.

[24] Armas, O., S. Martínez-Martínez, C. Mata and C. Pacheco. “Alternative method for bulk modulus estimation of Diesel fuels.” *Fuel* 167 (2016): 199-207.

[25] Ferrari, A. and Zhang T. “Influence of the injector setup on digital and continuous injection rate-shaping performance in diesel engine passenger cars.” *Energy Conversion and Management* 205 (2020): 112259.

[26] Kim, J., J. Lee and K. Kim. “Numerical study on the effects of fuel viscosity and density on the injection rate performance of a solenoid diesel injector based on AMESim.” *Fuel* 256 (2019): 115912.

[27] Salvador, F., M. Carreres, J. D. L. Morena and E. Martínez-Miracle. “Computational assessment of temperature variations through calibrated orifices subjected to high pressure drops: Application to diesel injection nozzles.” *Energy Conversion and Management* 171 (2018): 438-451.

[28] Ferrari, A., C. Novara, O. Vento, M. Violante and T. Zhang. “A novel fuel injected mass feedback-control for single and multiple injections in direct injection systems for CI engines” *Fuel,* 334 (2023): 126670

[29] Postrioti, L., Giacomo Buitoni, F. Pesce and C. Ciaravino. “Zeuch method-based injection rate analysis of a common-rail system operated with advanced injection strategies.” *Fuel* 128 (2014): 188-198.

[30] Bejan, Adrian. *Advanced engineering thermodynamics*. John Wiley & Sons, New York, 2016.

[31] Ferrari, A., C. Novara, E. Paolucci, O. Vento, M. Violante and T. Zhang. “Design and rapid prototyping of a closed-loop control strategy of the injected mass for the reduction of CO2, combustion noise and pollutant emissions in diesel engines.” *Applied Energy* 232 (2018): 358-367.

[32] Ferrari, A. and O. Vento. “Influence of Frequency-Dependent Friction Modeling on the Simulation of Transient Flows in High-Pressure Flow Pipelines.” Journal of Fluids Engineering-transactions of The Asme 142 (2020).

[33] Catania, A.E., Ferrari, A. and Manno, M., 2009, “Development and Application of a Complete Multijet Common-Rail Injection-System Mathematical Model for Hydrodynamic Analysis and Diagnostics”, *ASME J Eng. Gas Turb. Power*, 130(6), pp. 062809-1:13.

[34] Jin, Z., Vento, O., Zhang, T., Ferrari, A., Mittica, A., Ouyang, L., and Tan, S. (March 4, 2021). "Numerical-Experimental Optimization of the Common-Feeding Injection System Concept for Application to Light-Duty Commercial Vehicles." ASME. *J. Energy Resour. Technol*. December 2021; 143(12): 122304. https://doi.org/10.1115/1.4050133

[35] Blackburn JF, Reethof G, Shearer JL. “Fluid power control”. MIT Press; 1960.

[36] Payri, R., F. Salvador, M. Carreres and J. D. L. Morena. “Fuel temperature influence on the performance of a last generation common-rail diesel ballistic injector. Part II: 1D model development, validation and analysis.” *Energy Conversion and Management* 114 (2016): 376-391.

[37] Ferrari, A.. “Fluid dynamics of acoustic and hydrodynamic cavitation in hydraulic power systems.” *Proceedings of the Royal Society A: Mathematical, Physical and Engineering Sciences* 473 (2017).

[38] McCloy, D. and H. Martin. "Control of Fluid Power : Analysis and design", 2nd edition. Ellis Horwood Limited 1980.

[39] Nurick WH. 1976, “Orifice cavitation and its effect on spray mixing.” J. Fluids Eng. 98, 681–689.

[40] Payri, R., J. M. García, F. Salvador and J. Gimeno. “Using spray momentum flux measurements to understand the influence of diesel nozzle geometry on spray characteristics.” *Fuel* 84 (2005): 551-561.

[41] Zhao, Jianhui, L. Grekhov and Peng-fei Yue. “Limit of Fuel Injection Rate in the Common Rail System under Ultra-High Pressures.” *International Journal of Automotive Technology* 21 (2020): 649-656.